REMOTE SENSING AND GIS-BASED ANALYSIS OF CAVE DEVELOPMENT IN THE SUOIMUOI CATCHMENT (SON LA - NW VIETNAM)

L.Q. Hung, N.Q. Dinh
Department of Remote Sensing and Geomatic, Research Institute of Geology and Mineral Resources, Thanhxuan, Hanoi VIETNAM
O. Batelaan
Department of Hydrology and Hydraulic Engineering, Vrije Universiteit Brussel, Pleinlaan 2, 1050 Brussels BELGIUM
V.T. Tam
The VIBEKAP Project, Research Institute of Geology and Mineral Resources, Thanhxuan, Hanoi VIETNAM
D. Lagrou
VITO, Boeretang 200, 2400 Mol BELGIUM

Integration of remotely sensed imagery with ground surveys is a promising method in cave development studies. In this research a methodology was set up in which a variety of remote sensing and GIS techniques support cave analysis in the tropical karst area of the Suoimuoi catchment, NW Vietnam. In order to extract the maximum information from different remotely sensed data, the hue invariant IHS transformation was applied to integrate Landsat multi-spectral channels with the high resolution Landsat 7 ETM panchromatic channel. The resulting fused image was used, after enhancement, to visually and digitally extract lineaments. Aerial photos evaluated the extracted lineaments. Based on lineament density indices a fracture zone favorable for cave development is defined. The distance between caves and faults was investigated as well as the correspondence between the cave occurrence and the fracture zone.

During the last decade, Vietnam experienced a rapid economic growth. Sustainable growth, however, also requires an improvement in the quality of life. Rural water supply and sanitation are, therefore, priority issues for the Vietnamese government and of international donors. Since 1998, the Vietnamese-Belgian research project "Rural development in the mountain karst area of NW Vietnam by sustainable water and land management and social learning: Its condition and facilitation" (Masschelein & Swennen 1997) aims at increasing knowledge and expertise regarding the assessment and evaluation of karst systems in Son La and Lai Chau provinces (NW Vietnam). In this karst area, short supply of domestic water in the dry season and flooding in the rainy season are two of the main issues. Both problems can be better managed with better knowledge of the underground rivers and reservoirs. The project has gained a lot of information from several speleological expeditions, organized by the Research Institute of Geology and Mineral Resources, Belgian Geological Survey, Belgian-Vietnamese Karst and Cave Association, and the Speleological Association of the University of Leuven (Dusar *et al*. 1994; Coessens *et al*. 1996; Mrose *et al*. 1998; Spekul *et al*. 2000). During three expeditions, 129 caves and 35 km of cave development have been surveyed.

The main purpose of the study is to examine the relationship between the development of caves and the tectonic structures in the karst area of Son La. The tools for this study have been remote sensing for fault and lineament extraction and GIS spatial analysis of cave passages corresponding with these faults and lineaments.

The study area, the Suoi Muoi River catchment, is situated northwest of the city of Son La, between longitude 103°33' E and 104°00' E and latitude 21°20' N and 21°29' N, covering 284 km² (Fig. 1). The population of the Son La province is 650,000 inhabitants, resulting in an average density of 48 inhabitants/km². Natural hazards, droughts and floods are frequent threats to daily life.

The Son La karst area is part of the Son La-Thuan Chau karst highland, a mountain range extending over 300 km in NW-SE direction and with an average width of 10-30 km. The karst landscapes include the absence of permanent surface flow, closed depressions, caves, the existence of large springs, and the presence of sinkholes into which entire streams, like the Suoimuoi River, disappear underground. In the Suoimuoi catchment, the karst landscape occurs mainly in the central part and stretches from northwest to southeast, averaging 10 km wide and ranging from 500-850 m high. The landscape is characterized by a peak cluster morphology (*cf.* Chinese Fengcong), blind valleys, deep dolines, narrow valleys, chained sharp peaks and many swallow holes exiting underground into caverns. In the middle part of the area, mainly peak forest landscape dominates with residual karst peaks and tower karst, which emerge here and there above the dissolution-erosion valleys (Tuyet 1998).

Vietnam has a humid tropical climate, heavily influenced

**Figure 1.
Map of study area, indicating the Triassic ($T_{2a}dg_1$ and $T_{2a}dg_2$), Carboniferous (C_3-P_{1bd}), Devonian (D_2bp_1, D_2bp_2, D_2bp_3) and Cambrian (E_3hr) karst formations, mapped cave locations and faults in the Suoimuoi catchment, digitized from geological map (Hop 1997).**
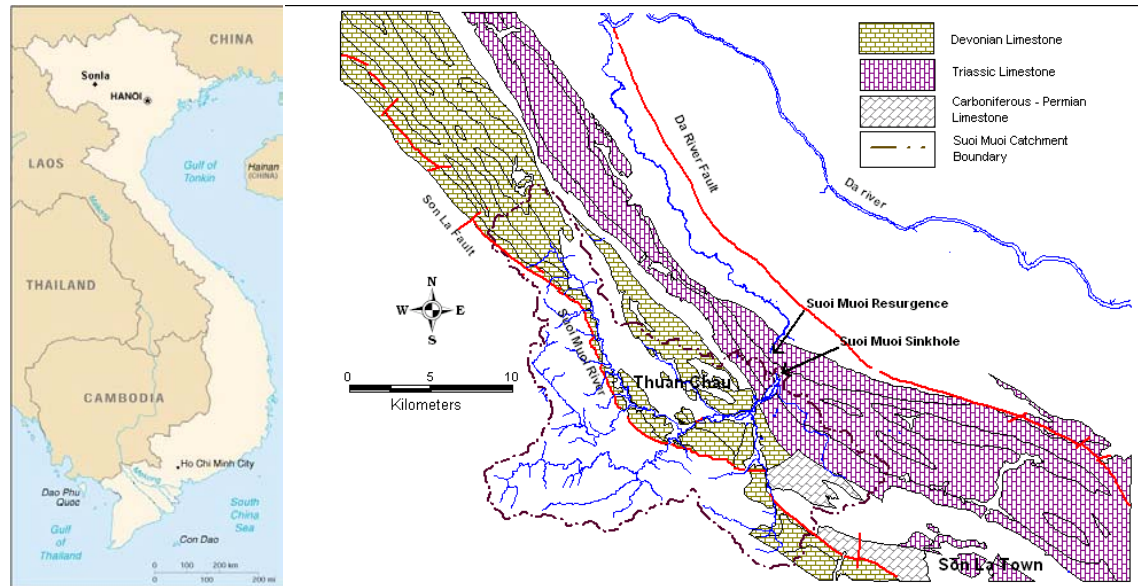
by the monsoon regime and characterized by two seasons: a hot and rainy summer and a colder and dry winter (Dieu 1992). In Son La, the annual mean temperature is 21°C, maximum and minimum recorded temperatures are 40°C and 1°C, respectively. The average humidity of the air is 80%, but may drop in winter to an all-time low of 6%. Eighty-five percent of the 1413 mm mean annual rainfall occurs during the rainy season (from April to September).

GEOLOGY

The Son La-Thuan Chau karst area consists mainly of two sub-areas. The southwestern parts are composed of karst water-bearing carbonate rocks of Paleozoic age, Banpap (D_2bp) and Early Permian-Carboniferous Chienpac (C-P_1cp) Formations. The northeastern part is of Middle Triassic age with the Dong Giao Formation (T_2dg). Table 1 presents a summary of the stratigraphic description of the carbonate rocks in the area. In the Suoimuoi catchment, karst occurs in limestones and dolomites of Late Cambrian, Middle Devonian, Carboniferous - Early Permian and Middle Triassic age. These carbonates have a favorable composition, texture, and structure for karstification (Hung 2001).

Many different tectonic phases and neotectonic movements have intensively affected these rocks. The present Son La karst highland is dissected by NW-SE, SW-NE, sublatitudinal, and submeridianal trending faults. The NW-SE fault system resulted from the collision of continental crust in the Precambrian. The region then was affected by NW-SE oriented folding due to Indosinian closure of the Paleotethys, starting in Late Permian and culminating during Middle Triassic. All the deposits were finally uplifted during the Neogene Himalayan collision event (Tri *et al*. 1977; Tri & Tung 1979; Tien *et al*. 1991). A series of sub-parallel strike-slip faults can be recognized in the Son La fault zones. Furthermore, Son La town is

located on the active Tuan Giao-Son La seismic zone where many destructive earthquakes with intensities of up to 7.0 on the Richter scale have been recorded in this zone. Damage to property has included rockfalls, ground cracking, and landslides (Dusar *et al*. 1994). Along the NW-SE faults, the width of fractured zone ranges from 1 - 2 km.

The SW-NE fault system is younger than the NW-SE one. The continuous tectonic activity in the Son La region accompanied by strong uplift and associated tilting towards the Da River valley to the east, has resulted in the destruction of the Miocene-Pliocene peneplane surface and the creation of deeply incised valleys. This system modifies the block structures formed by the faulting. These SW-NE transform faults are discontinuous. The width of fractured zone ranges from 800-1200 m (Hop 1997).

The development and characteristics of karst depends on many interacting factors such as: composition, texture and solubility of carbonate rocks, folding, faulting, neotectonic activity, quality and quantity of water, availability of CO_2 gas from various sources, character of vegetative cover, as well as environmental conditions, including human impacts. Tam *et al*. (2001) concluded that the karst groundwater aquifers in the Suoimuoi catchment are determined by fractured/fissured media whilst the cavern conduits, although abundantly occurring in the region, act as groundwater galleries and/or conveyers.
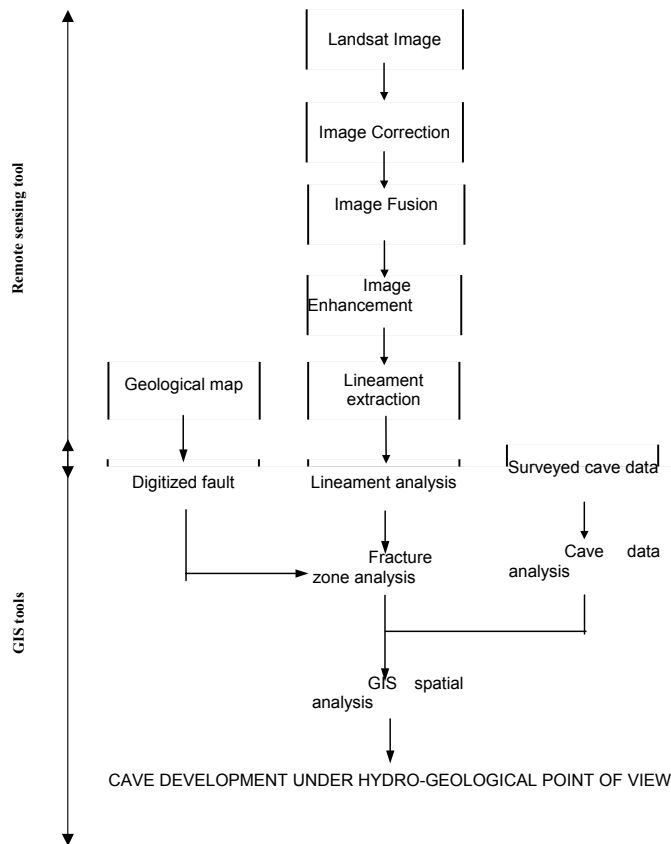
DATA

A Landsat 7 ETM satellite image of February 27th, 1999, has seven multispectral bands and additionally a panchromatic band of 15 m resolution. Additionally, 36 aerial photographs, along four flight lines, were available for January 1975 and January 1999. The nominal scale of the aerial photographs is 1:33,000. All photos were scanned with a resolu-

Table 1.
A summary of the stratigraphic column for the Suoimuoi catchment. The Triassic (T₂adg₁ and T₂adg₂), Carboniferous (C₃-P₁bd), Devonian (D₂bp₁, D₂bp₂, D₂bp₃) and Cambrian (E₃hr) karst formations have been indicated in bold.

Age			Code	Thickness (m)	Description
Cenozoic	Quarternary	Holocene	Q	10-15	Alluvium and deposit of temporal flows include cobbles, gravels, mixed composition, badly rounded, sand and clay upward.
Mesozoic	Cretaceous	Middle	K_2yc_3	300-400	Upper Yenchau sub-Formation: sandstone, gravelstone and calcareous sandstone, red color.
			K_2yc_2	600-900	Middle Yenchau sub-Formation: sandstone, siltstone and some lenses of calcareous conglomerate and gravelstone, red color
			K_2yc_1	350-500	Lower Yenchau sub-Formation: conglomerate with gravelstone lenses, light grey color.
	Triassic	Late	$T_{3n-r}sb$	400	Suolbang Formation: lower: dark grey siltstone, sandstone, calcareous shale, siliceous limestone lenses, fossil-bearing tufaceous sandstone. Upper: siltstone, dark grey sandstone with fine sandstone rich in organic calcareous clay and thin lenses of coal.
		Middle	$T_{21}mt_3$	350-400	Upper Muongtral sub-Formation: shale, dark grey oolitic siltstone, sericite sandstone with moderate to thick bedding and calcareous sandstone. Rich in fossils.
			$T_{21}mt_2$	700-900	Middle Muongtral sub-Formation: calcareous claystone, limestone breccia in block structure or thick bedding.
					Upper Namthan sub-Formation: lower part: black shale, thin bedding siliceous limestone. Middle part: light grey, white limestone, irregular bedding, and clayish intercalations. Upper part: limestone, dolomitized limestone, thick bedding and rich in fossils.
			$T_{21}mt_1$	600-1500	Lower Muongtral sub-Formation: lower part: thin layers of dark grey shale, porphyry basalt and continental basalt.
					Lower Namthan sub-Formation: lower part: dark-to-light grey, partly dolomitized limestone, thick bedding and rich in fossils. Middle part: sandstone, sandy siltstone, gravelstone and fauna fossils. Upper part, marl, black-coaly shale and flora fossils.
			T_2adg_2	1100	**Upper Dong Giao sub-Formation**: lower part: dark grey limestone intercalated with the light grey, irregularly dolomitized, thick bedding and rich in fossils. Upper part: light grey limestone, partly domomitized, thick bedding to massive structure and rich in fossils.
			T_2adg_1	350-720	**Lower Dong Giao sub-Formation**: calcareous schist, siltstone, black oolite-limestone intercalations and upwards: dark grey clayish limestone, siliceous bituminiferous limestone, thin bedding and rich in fossils.
		Early	T_1tl	250-300	Taniac Formation: lower part: conglomerate with majority of basalt cobbles, tufaceous sandy cement, tufaceous sandstone and siltstone upwards. Upper part: siltstone, claystone with clayish limestone, oolite, wormlike textured limestone and rich in fossils.
			T_1vn	250-300	Viennam Formation: lower part: alkaline olivine basalt, trachybasalt, plagiobasalt and green basalt. Upper part: rhyolite, trachydacite, trachyrhyolite and lava breccia.
					Conoi Formation: lower part: sandy tufaceous siltstone, claystone with arkose sandstone and limestone laminations. Upper part: siltstone, sandstone, calcareous claystone with clayish limestone laminations, oolite, wormlike textured limestone and rich in fossils.
Paleozoic	Permian	Middle	P_2yd	150	Yenduyet Formation, lower part: banded siltstone, schist fereous allite and tufaceous sandstone. Middle part: organic oolite limestone, dark grey siliceous deposit and rich in fossils. Upper part: black schist with siliceous intercalations, limestone and rich in fossils.
			P_2T_1nm	250-400	Camthuy Formation, lower part: porphyryte basalt, green basalt, dolomite breccia, tuff and clayish limestone lens. Upper part: laminations of tufaceous siltstone, few basalts and allite lenses.
					Nammuoi Formation: mafic and neutral extrusive rock with high magnesium. Low titanium, mainly: komatite, basaltkomatite, picrite basalt, boninite, okeanite and ankaramite.
	Carboniferous	Late	C_3P_1bd	600-770	**Bandiet Formation, lower part**: mafic extrusive rock, black siliceous deposit, tuff sandstone and coaly claystone. Upper part: dark grey limestone, schist laminations, limestone breccia, regular bedding to massive structure and rich in fossils.
					Chiengp ac Formation, lower part: light grey, fine grained limestone with organic limestone and dark spots, breccia, oolite, thick to massive structure and rich in fossils. Upper part: green grey limestone, thin bedding and rich in fossils.
	Devonian	Late	D_2bp_3	190-270	**Upper Benp ap Formation**: light grey limestone, thick bedding to massive structure, micro-grained and partly dolomitized limestone, clayish limestone, thin layers of siliceous limestone, contains fossils.
		Middle	D_2bp_2	150-250	**Middle Benp ap Formation**: dark grey and ash-grey limestone, thick bedding to massive structure, clayish oolite limestone with thin bedding, grayish limestone intercalations, irregularly calcitized and rich in fossils.
		Early	D_2bp_1	350	**Lower Banp ap Formation**: dark grey, black and partly dolomitized limestone, siliceous limestone, clayish limestone, thin bedding and rich in fossils (corals).
			$D1np$	300	Nampia Formation: quartz-sericite schist, sericite-quartz-chlorite schist and thin-bedded sandy siltstone with lenses of sandstone.
	Ordovician	Early	O_1ds	350-370	Dongson Formation, lower part: quartizitised arkose sandstone and sandstone laminations. Upper part: quartz-sericite schist, sericite sandstone intercalations, contains fossils.
	Cambrian	Late	E_3hr	400-720	**Hamrong Formations, Lower part**: pale grey, fine limestone, partly dolomitized limestone, oolite and clayish limestone. Upper part: clayish limestone, schist with few calcareous siltstones and sandstones, contains fossils.
		Middle	E_2sm	730-850	Songma Formation, divided into 3 parts including: conglomerate, coaly schist, mica-quartz-sericite-chlorite, quartz-feldspars-biotite, schist, green schist, amphibolite schist, quartzitic sandstone and limestone lenses.
Late Proterozoic			$PR_3-E_1nc_3$	500-550	Upper Namco sub-Formation: mica-quartz, mica-quartz-sericite, chlorite schist with quartzitic, siliceous sandstone and intercalations. Upper part: quartz-sericite-chlorite with quartzitic sandstone intercalations.
			$PR_3-E_1nc_2$	800-1000	Middle Namco sub-Formation: lower: mica-quartz-garnet schist, biotite-staurolite schist (andalusite) with micaceous, mica-quartz intercalations. Upper: quartz-feldspar-biotite schist containing garnet with quartzite, sericite, siliceous intercalations.
			$PR_3-E_1nc_1$	400-450	Upper Namco sub-Formation, lower part: biotite-quartz schist bearing cordierite and staurolite with some black siliceous schist. Upper part: micaceous-quartz and quartz-sericite-chlorite schist.

```
Landsat Image
    ↓
Image Correction
    ↓
Image Fusion
    ↓
Image
Enhancement
    ↓
Lineament
extraction
```

Geological map

Digitized fault   Lineament analysis   Surveyed cave data

Fracture
zone analysis   Cave   data
analysis

GIS   spatial
analysis

CAVE DEVELOPMENT UNDER HYDRO-GEOLOGICAL POINT OF VIEW

Remote sensing tool

GIS tools

Figure 2. Flow-chart for RS and GIS based methodology of cave development analysis.

tion of 600 dpi, resulting in digital aerial images with high-resolution features. Reference data available over the study area comprise the geological map, a digital elevation model (DEM) with a spatial resolution of 20 m and four 1:50,000 scale topographic maps with UTM projection (zone 48N).

The geological map (Hop 1997) provided a data layer indicating the faults and lineaments. The caving data consist of the description of the mapping of 97 caves in Suoimuoi catchment and direct surroundings as reported from caving expeditions (Dusar *et al*. 1994; Coessens *et al*. 1996; Mrose *et al*. 1998). Using, the dataset, a cave database was built using CaveTools (Szukalski 2001), ArcView, and MS-Access.

Methodology

Remote sensing

The combination of remote sensing and GIS provides a set of tools for cave development analysis. In Figure 2, the major analysis steps for cave development based on analyzed Landsat ETM and a cave database are given. In a first step, the Landsat image was geometrically corrected, followed by image fusion. Image fusion is defined as combining two or more different images to form a new image with a certain algo-

rithm (Carper *et al*. 1990). It is clear that the selection of an image fusion approach depends on the desired application (Zhang *et al*. 1999). Our purpose was to integrate images from different sensors to facilitate visual interpretation. For this purpose, pixel-based statistical/numerical or color related fusion techniques are an appropriate tool. Statistical/numerical fusion uses the statistics of individual image bands for correlation analysis. The color related fusion methods were used here and deal with the transformation between display-device and perceptual color spaces. The most popular color related technique is the transformation of image data from the red-green-blue (RGB) color space to the intensity-hue-saturation (IHS) space and vice versa (Fig. 3).
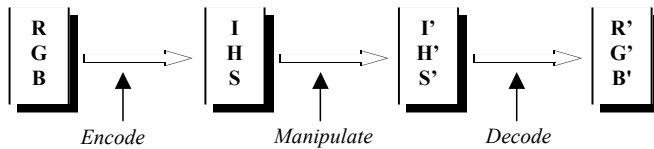
The intensity relates to the brightness, hue represents the dominant wavelength, while the saturation is defined by the purity of the color. In the first transformation step, a multispectral RGB composite image was encoded to the IHS space. In the manipulation stage, intensity was substituted by another image or "replacement intensity". In this stage, saturation can be enhanced by multiplying it with a scale factor (e). During fusing of the two datasets, the saturation enhancement scale factor "e" is controlled in order to reduce over-range pixels. When multispectral channels are fused with the panchromatic band, saturation can be enhanced up to e=3 (Ha 2001). Care should be taken with the enhancement of hue because it may result in spectral distortions (Schetselaar 2001). The principle of image fusion can be written as a single transformation, which allows control on the enhancement and over-range with respect to the faces of the RGB cube and limits hue distortions (Schetselaar 2000):

$$\begin{pmatrix} R \\ G \\ B \end{pmatrix} = \left(\frac{I'}{I} \right) \begin{pmatrix} \frac{1}{3}+\frac{2}{3}e & \frac{1}{3}-\frac{1}{3}e & \frac{1}{3}-\frac{1}{3}e \\ \frac{1}{3}-\frac{1}{3}e & \frac{1}{3}+\frac{2}{3}e & \frac{1}{3}-\frac{1}{3}e \\ \frac{1}{3}-\frac{1}{3}e & \frac{1}{3}-\frac{1}{3}e & \frac{1}{3}+\frac{2}{3}e \end{pmatrix} \begin{pmatrix} x_1 \\ x_2 \\ x_3 \end{pmatrix}$$

$$I = (1/\sqrt{3})(x_1 + x_2 + x_3)$$

Where (x_1, x_2, x_3) is the multispectral feature vector of a pixel, I is the intensity of that pixel, I' is the replacement intensity, e is saturation enhancement. The technique can be applied to fuse images from a single sensor, or multisensor data, or image data with ancillary data, like geophysical, geochemical, thematic data, and data compiled from fieldwork (Harris *et al*. 1990; Schetselaar 2000). By fusing multispectral channels with high spatial resolution channels, enhancements are expected with respect to geographical features, boundaries between different lithological units and the relationship between the multispectral and high spatial resolution information.

In the next step of remote sensing analysis, lineaments were detected and extracted (Hung 2001). A lineament is a

Figure 3: The IHS principle (Lillesand and Kiefer 1994).

Table 2: Some major characteristics of visual and digital lineament extraction.

Visual processing	Digital processing
- Relatively higher quality if image quality is low	- Relatively higher quality if image quality is high
- Higher quality if the research area has high complexity	- Lower quality if the research area has high complexity
- Strongly depends on human experience	- Strongly depends on software functionality
- Slow	- Fast
- Easy to distinguish the type of lineament	- Cannot distinguish the type of lineament
- Simple but subjective method	- Complex but objective method

mappable linear or curvilinear feature of a surface whose parts align in a straight or slightly curving relationship. They may be an expression of a fault or other line weakness. The surface features making up a lineament may be geomorphological (caused by relief) or tonal (caused by contrast differences). Straight stream valleys and aligned segments of a valley are typical geomorphological expressions of lineaments. A tonal lineament may be a straight boundary between areas of contrasting tone. Differences in vegetation, moisture content, and soil or rock composition account for most tonal contrast (O'Leary *et al.* 1976). In general, linear features are formed by edges, which are marked by subtle brightness differences in the image and may be difficult to recognize.

Directional and non-directional filters have been developed to enhance edges in images. Laplacian filters are non-directional filters because they enhance linear features having almost any orientation in an image. The exception applies to linear features oriented parallel with the direction of filter movement; these features are not enhanced. Directional filters are used to enhance specific linear trends in an image. Sabins (1997) shows some major directional filters that can enhance any specific direction. Since image noise can create linear features, edge enhancement is strongly dependent on the pre-processing of the images.
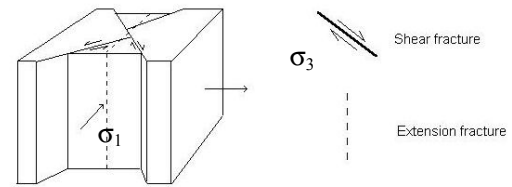
In the last remote sensing analysis step, lineaments are extracted visually or digitally (automatically). Both methods have certain advantages and disadvantages (Table 2). Because of the complexity of the process, only a few automatic lineament extraction schemes exist and most lineament extractions still depend on the researcher's experience. In order to study the tectonic fracture zone in Suoimuoi catchment, both visual and digital lineament extraction were applied. The digital extraction used Laplacian and directional filters to enhance the lineaments; consequently the enhanced image was converted to Boolean images using different threshold values. Lineaments from these images were extracted by OCR-tracing software, combined, and further processed by lineament specific software (Hung 2001).

STRUCTURAL DEFORMATION

Through brittle deformation, two mechanisms or modes of propagation, shear and extension, generate fractures. Frequently, the shear fractures occur as a conjugate pair and the extension fractures bisect the acute angle in pair. The extension features are oriented parallel to the direction of the maximum compressive stress (σ_1), and perpendicular to the

Figure 4: Stress orientation and corresponding types of fractures.

minimum stress (σ_3) (Fig. 4). As a result of propagation mode, the apertures of the extension fractures tend to be larger than those of shear fractures. Groundwater flow may be more significant along the extension fractures. Fernandes and Rudolph (2001) concluded that tectonic activities, which result in brittle deformation, generate: 1) shear fractures that remain under compression and are not very transmissive; and 2) more permeable extension structures tend to be associated with wide-aperture fractures. The recognition of these extension fractures would be valuable for groundwater resources development. Lineament analysis may be the most effective method to map these types of features.

By understanding the orientation of the stress field that generated the structures in the study area, it is possible to evaluate which lineaments can be associated with mostly shear fractures or conjugated faults and which with extension fractures. Figure 4 depicts the stress field and the general position in space of the shear and extension fractures that are generated by a strike-slip tectonic regime.

CAVE ANALYSIS

In order to investigate the relationship between the occurrence of caves and geologic structures, a spatial GIS analysis was performed using the ArcView software (ESRI 1996). In the first step, an ArcView shape file, indicating the cave entrances, was transformed to a grid by using the "Find distance" function. Each resulting grid cell with a spatial resolution of 10 m bears the value indicating the distance between itself and the nearest cave. Then by reclassification, a buffer

zone with a radius of 20 m or two grid cells is defined around the cave grid cell. The purpose of the buffer zone around the cave is to cover the area of the cave entrance or doline as well as to take into account the effect of errors in locating the caves (Dinh 2001).

In the second step, the digitized fault sheet from the geological map and the visually extracted lineament maps as polyline shape files are transformed to grids with a resolution of 10 m. Similar to the cave map, a map showing the distance to the nearest fault or lineament was created. The resulting fault distance zone map was reclassified in 6 distance zones, where each of the first 5 zones have a width of 100 m adding up to 500 m, while the last zone covers the remaining area. The maximum buffer zone was defined as 500 m since this is half of the width of the commonly found fractured zone bordering a fault (Hop 1997). In the third step, statistics for each zone were calculated. The ArcView Spatial Analyst "Histogram by Zone" function was used to identify the percentage of cave pixels that fall within each buffer zone bordering the faults.

In the final step, the comparison of the direction of cave development and fault direction was performed. Although each cave has its own properties, characterized by its own unique speleogenetic history, general directions can be observed. Classification of direction was based on the maximum length of the cave in a certain direction; that means the cave is considered to be developed in the direction along which most cave passage developed. One can determine the direction of the cave by using a rose diagram, a built-in function of the COMPASS software (Fish 2001).

Results and discussion

Lineament and fracture zone analysis

The results of the visual and digital lineament extraction, after directional and non-directional enhancement of the fused image, are given respectively in Figures 5a and 5b. Randomly selected visually extracted lineaments were visually compared with observed lineaments from the high-resolution aerial photos to improve the visual selection procedure. The DEM was also used to verify the location of the extracted lineaments. The lineaments resulting from visual processing are relatively continuous lines. Since visual lineament extraction selects lineaments based on morphological characteristics, they correspond well to the mapped faults from the geological map (Fig. 1). However, the visual extraction results in more lineaments and with a higher spatial accuracy than faults present in the geological map. The digitally extracted linear features are considered as lineaments if they are longer than 100 m (6 pixels). Two lineaments will combine into one, if they have a maximum difference in direction of 3° and/or if the space between them is less than 45 m (3 pixels). The resulting digitally extracted lineaments are still relatively short compared to the visual lineaments, but they have a high density (Fig. 5b). Non-tectonic linear features (roads, etc.) and, especially, the shadow in the image are the cause of this high density. In visual
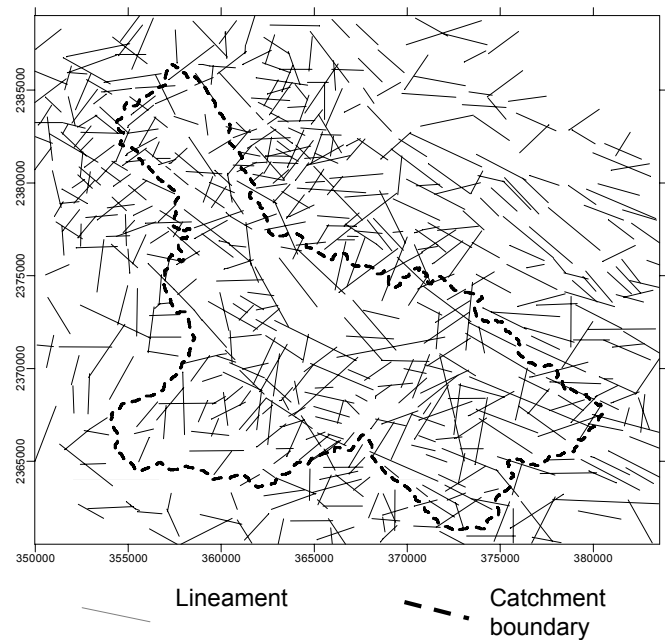

Figure 5a: The result of visual lineament extraction from the fused, transformed Landsat images.
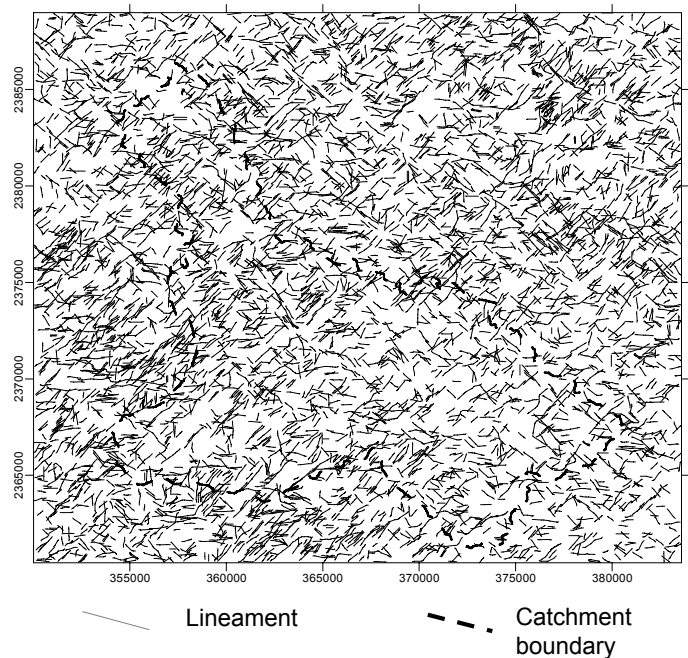
Figure 5b: The result of digital lineament extraction from the fused, transformed Landsat images.

processing shadow is much less of a problem.

In order to define the fracture zone, the map with digitally extracted lineaments was used to calculate the density of lineaments in the Suoimuoi catchment under the hypothesis that

99 — Contour line
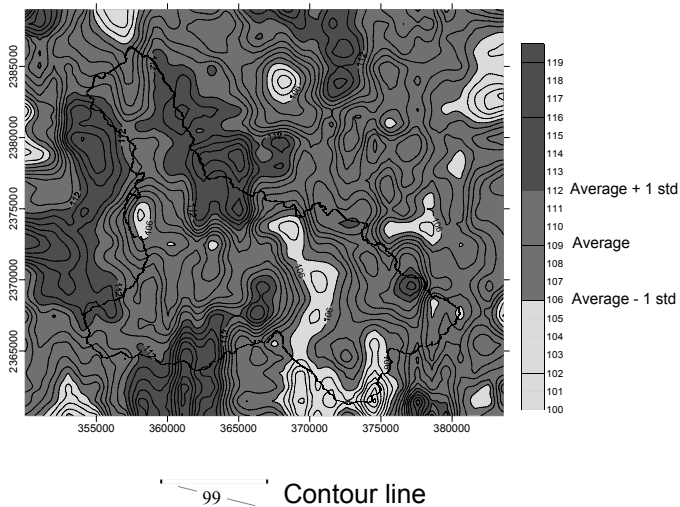
Figure 6: Contour map of the average of lineament length (meters) per km².

Catchment boundary

Figure 7: Contour map of the ratio between the number of lineament intersections and the number of lineaments per km².

a higher density of lineaments indicates a higher intensity of deformation. The most common method is to calculate lineament density as the number of lineaments per unit area (n/km²), or as the number of lineament intersections per unit area (n/km²), or as the total length of lineaments per unit area (m/km²). In order to avoid the effect of non-tectonic lineaments here, two other indices are used: the average of the lineament length per km² and the ratio between number of intersections of lineaments and the number of lineaments per km². These lineament density indices are calculated for a raster with a grid cell resolution of 1 km² and can be reclassified into ranges of values and presented as an isopleth map (Figs. 6 and 7). The major statistical characteristics of the two density maps are listed in Table 3.

Since the Suoimuoi catchment can be considered as a homogeneous tectonic region, the fracture zone can be defined on basis of the statistical characteristics of the two indices: average length of lineaments and ratio between number of intersections of lineaments and the number of lineaments per km². In zones with a low value of these indices, caves cannot develop. In zones with a very high density, rock stability is too low for cave development. Therefore, the fracture zone is defined as the zone where the two indices have a value between the average plus and minus one standard deviation.

Two main types of conjugate fracture patterns are recognized for the Suoimuoi catchment, depicted by the diagrams in Figure 8a. Hop (1997) supposed that both fracture types (E-W and NW-SE) generated faults (shear fractures) and extensional fractures that affected the rocks from Precambrian up to Middle Triassic. The E-W fracture type is accompanied by shear fractures with a NW-SE and NE-SW direction and extension fractures with a sub-E-W direction. The NW-SE fracture type is accompanied by shear fractures of sub-N-S and sub-E-W direction and extension fractures with a NW-SE direction. The correspondence of the NW-SE shear and extension direc-
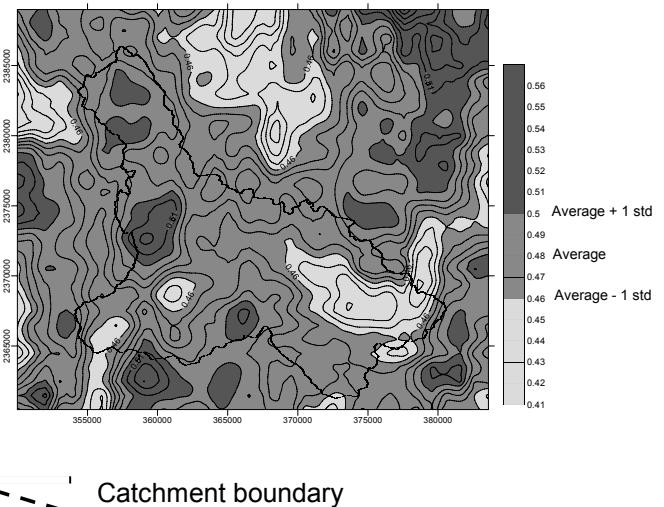
Table 3: Statistical characteristics of digitally extracted lineaments.

Lineament index	Statistical characteristics			
	Max	**Min**	**Average**	**Standard deviation**
Total length (m)	119526	11285	75486	21231
Intersection	521	46	331	95
Ave. length (m)	120	99	109	3
Inter/number	0.56	0.41	0.48	0.02

tions and the E-W correspondence of shear and extension directions, make these two directions most favorable for groundwater development.

In Figure 8b, the rose diagram is given for the visually extracted lineaments. It is clearly observed that the directions correspond to the results of Hop (1997) as given in Figure 8a. The density of the lineaments differs. The visual extraction results in more sub-N-S and sub-E-W lineaments than in Figure 8a. Figure 8c shows the rose diagram for the digitally extracted lineaments. The very high density of NW-SE and NE-SW lineaments in this figure is due to additional lineaments caused by the effect of shadow in the image. The densities of the sub-N-S and sub-E-W lineaments are, therefore, relatively reduced.

CAVE DEVELOPMENT STUDY BASED ON LINEAMENT ANALYSIS

Figure 1 shows the location of the 97 mapped caves. The caves cluster in the southeast and northwest of the catchment. This is partly due to the fact that the cave mappings were not performed systematically over the area due to the inaccessibility of the terrain, e.g. in the northern central karst part. From Figure 1, it is observed that the occurrence of the caves corresponds to the areas with a relatively high number of intersec-
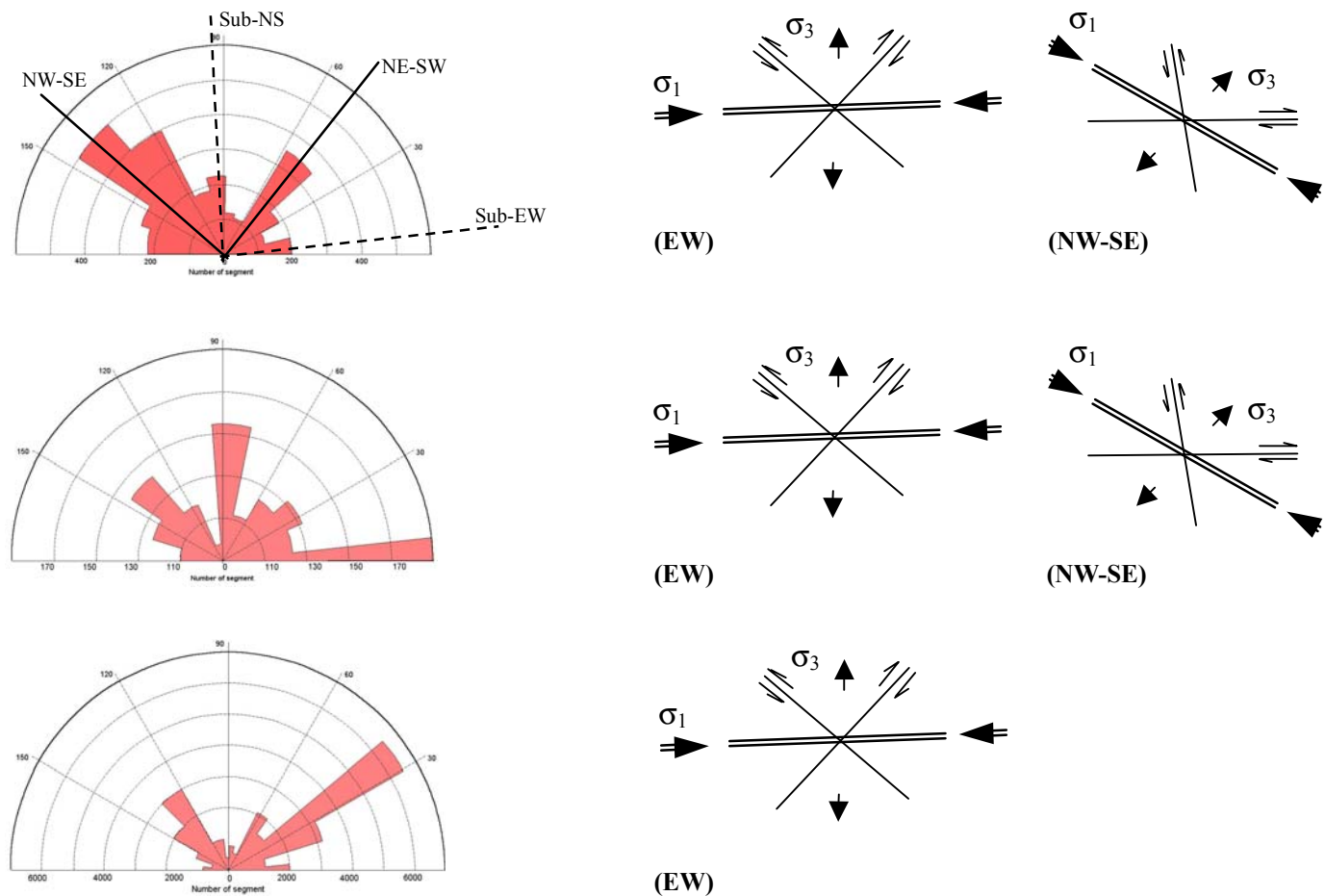
Figure 8a (top): Rose diagram depicts the distribution of lineaments on geological map (Hop 1997). Also shown are the orientations of shear and extension fractures.
Figure 8b(center): Rose diagram of visually extracted lineaments and related directions of shear and extension fractures.
**Figure 8c (bottom): Rose diagram of digitally extracted lineaments and related directions of shear and extension fractures.**

tions of NW-SE, NE-SW, and E-W faults. In the southeast the caves occur favorably at the contact of limestone and non-limestone formations. In the narrow karst band running from northwest to southeast cave development is not favorable since the Late Cambrian formations only contain thin carbonate lenses, which are partly dolomitized and separated by conglomerates and metamorphic rocks.

In Figure 9a, the results of the analyses of the distance between the caves and the faults, which were derived from the geological map, are presented. The bar chart indicates the percentage of caves occurring within a certain distance zone from the faults. It is concluded that more than 80% of caves are situated within the fractured zone (< 500 m), pointing to a high likelihood of tectonic control in the development of the caves. The fault map shows only faults that play a controlling factor to the regional structure and the faults that are not covered by the Quaternary sediments. If non-regional and non-superficial faults had been included, likely a higher percentage of cave-fault correspondence would have been achieved. In Figure 9b, the diagram shows the results from distance analyses of the

cave to the visually extracted lineaments. Ninety-seven percent of the caves are located within 500 m of the fractures. Lineaments represented all the features caused by tectonic activities, not only faults but also folds and edges, which may explain why a higher percentage of caves located close to the lineaments compared to the faults.

In Figure 9c, the results are shown from the analysis of the direction of cave development and the fault direction. From the caves that have been surveyed, 58% of the caves developed in NW-SE direction, corresponding to the most pronounced regional tectonic direction. Nineteen percent of the caves developed along high density SW-NE lineament direction, while only 15% and 8% of the caves developed, respectively, along N-S and W-E directions. Most of the active caves, which have developed along NW-SE direction, have horizontal passages or very slightly inclined passages, while most of the caves developed along NE-SW direction have inclined passages (Dusar *et al.* 1994). The inclination of those caves somewhat follows the dipping of carbonate rocks. In those cases, the bedding planes may also provide routes for groundwater
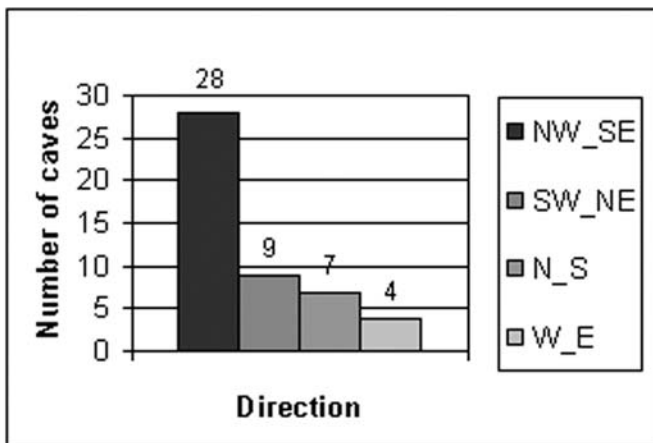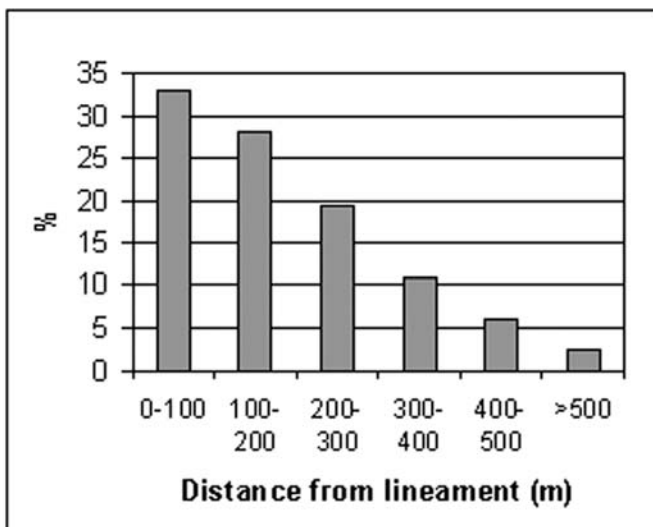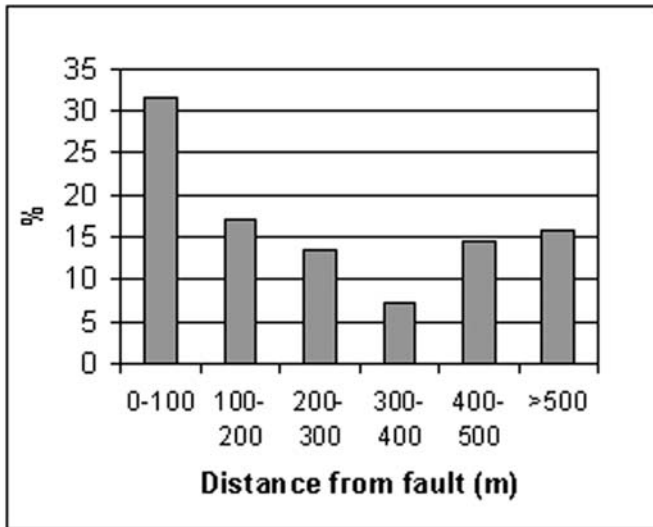
Figure 9: Bar graph showing the number of mapped caves (a - top) with respect to fault distance, based on faults from the geological map (Hop 1997), (b - center) with respect to lineament distance, based on map of visually extracted lineaments, (c - bottom) versus main fault direction.

eaments. The crosshatched area in Figure 10 is the most favorable fracture zone for cave development since it is the overlap of the two extracted fracture zones of Figures 6 and 7. Most caves are located in the favorable fracture zone. In the central-southeast part, some caves do fall outside the favorable fracture zone; however, they have developed on the contact of limestone and non-limestone formations. The absence of caves in the central-northern part of the karst belt can be explained from the fact that only a very small part of the area belongs to the favorable fracture zone. The favorable fracture zone in Figure 10 can be used to suggest zones for finding new caves in the Suoimuoi catchment.
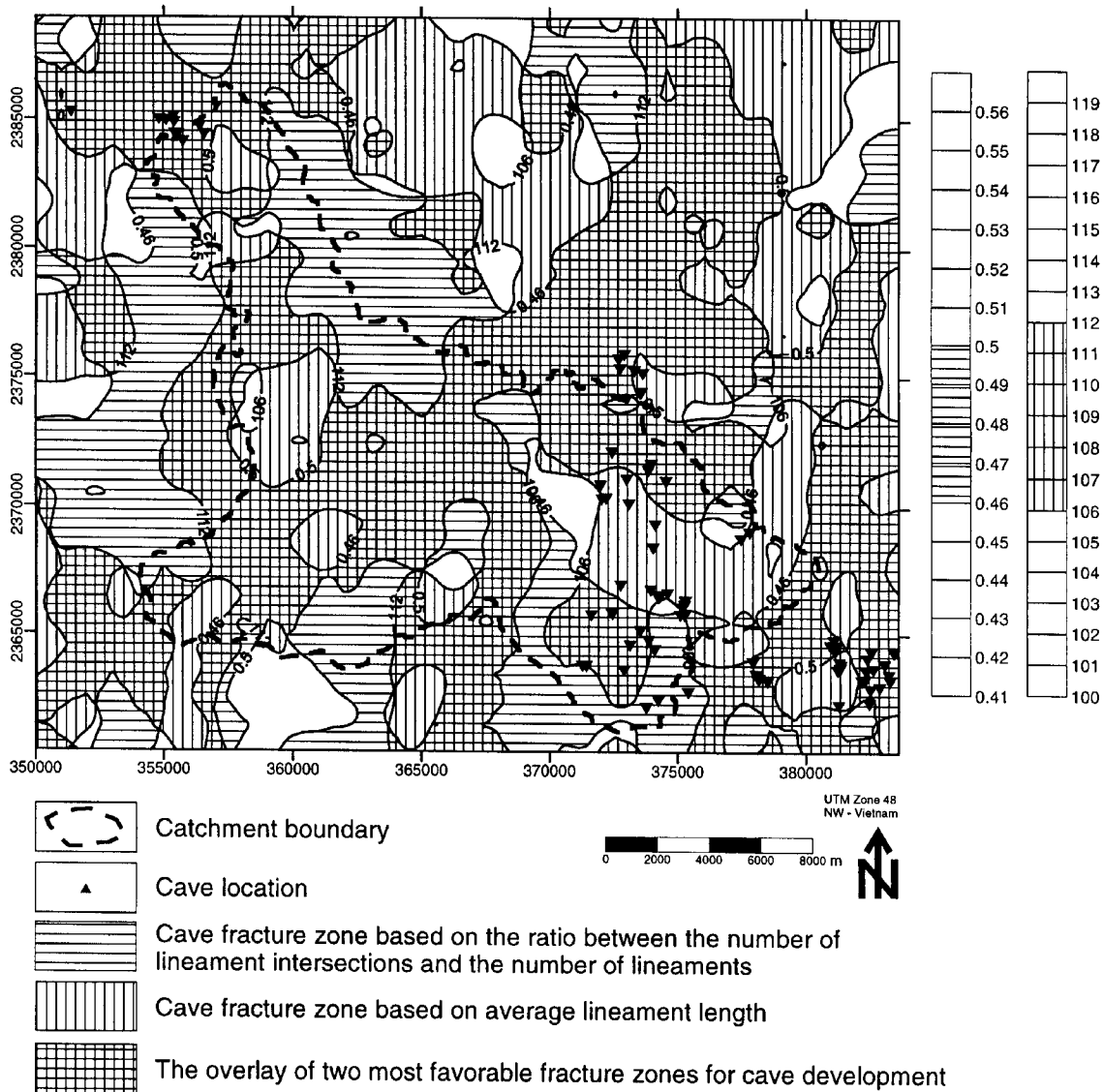
CONCLUSIONS

A methodology has been set up, involving remote sensing and GIS analysis to map, predict and explain the occurrence of caves in a tropical karst region. Based on a geologic analysis, it is concluded that tectonic activity was very strong in the Suoimuoi catchment. The tectonics resulted in a NW-SE dominated fault system.

The integration of Landsat 7 ETM imagery with high-resolution panchromatic data provided complementary information with respect to the discrimination of major geologic features and allowed lineament extraction in detail. A favorable fracture zone for cave development is determined through the analysis of the lineaments.

The cave correspondence with the fractured zone was very high. Outside the fractured zone caves occurred at the formation contact between limestones and non-limestones. The majority of the caves developed along the major structural NW-SE direction. It is suggested that the favorable fracture zone for cave development can be used to predict cave occurrences.

movement. However, in such cases movement is often controlled by fracture patterns and hydrological regimes.

Figure 10 combines density data for average lineament length, number of lineament intersections, and number of lin-

Figure 10. Overlay of the density map of average lineament length with the density map of the ratio between the number of lineament intersections and number of lineaments. The horizontal and vertical hatched areas are the fracture zones favorable for cave development. Overlain, the cross-hatched area is the most favorable fracture zone for cave development.

Catchment boundary

Cave location

Cave fracture zone based on the ratio between the number of lineament intersections and the number of lineaments

Cave fracture zone based on average lineament length

The overlay of two most favorable fracture zones for cave development

Hung and N.Q. Dinh. Finally the reviewers of the article are acknowledged for improving the text.

REFERENCES

Carper, W.J., Lillesand, T.M., & Kiefer, R.W., 1990, The use of intensity-hue-saturation transformations for merging SPOT panchromatic and multi-spectral image data: Photogrammetric Engineering and Remote Sensing, v. 56, p. 457-467.

Coessens, V., Deblaere, C., Lagrou, D., Masschelein, J., Tien, P.C., & Tuyet, D., 1996, Belgian-Vietnamese speleological expedition Son La 1995-1996: Cave investigation, a start for research on sustainable development, BVKCA, SPEKUL, RIGMR report, 63 p.

Dieu, N.T., 1992, Geography of Vietnam: Hanoi, The Gioi Foreign Languages Publishing House.

Dinh, N.Q., 2001, Cave database development, spatial analysis and 3D visualization with GIS, case study in Sonla - Vietnam [MSc thesis]: Vrije Universiteit Brussel, 114 p.

Dusar, M., Masschelein, J., Tien, P.C., & Tuyet, D., 1994, Belgian-Vietnamese speleological expedition Son La 1993, Professional Paper Belgian Geological Survey1994/4-N.271, 60 p.

Fernandes, A.J., & Rudolph, D.L., 2001, The influence of Cenozoic tectonics on the groundwater-production capacity of fractured zones: A case study in Sao Paulo, Brazil: Hydrogeology Journal, v. 9, p. 151-167.

Fish, L., 2001, COMPASS - software package for processing cave survey data, http://www.fountainware.com/compass/.

Ha, L.T.C., 2001, Integrating landsat ETM7, aerial photographs and field data for geological mapping - the Tabernas basin - Southeast Spain [MSc thesis]: ITC, 174 p.

Harris, J.R., Murray, R., & Hirose, T., 1990, IHS transform for the integration of radar imagery and other remotely sensed data: Photogrammetric Engineering and Remote Sensing, v. 56, p. 1631-1641.

Hop, N.D., 1997, Geological map of Thuan Chau - Son La (Vietnam): Hanoi, The Geological Survey of Vietnam, p. 600.

Hung, L.Q., 2001, Remote sensing based hydrogeological analysis of Suoimuoi catchment Vietnam [MSc thesis]: Vrije Universiteit Brussel, 87 p.

Lillesand, T.M., & Kiefer, R.W., 1994, Remote sensing and image interpretation: New York, John Wiley & Sons, Inc, 750 p.

Masschelein, J. & Swennen, R., 1997, Project proposal: Rural development in the mountain karst area of NW Vietnam by sustainable water and land management and social learning: Its conditions and facilitation, VIBEKAP documents, http://www.vub.ac.be/vibekap/.

Mrose, N., Van Baars, M., Coessens, V., Deblaere, C., Lagrou, D., Masschelein, J., Tien P.C., & Tuyet, D., 1998, Belgian-Vietnamese speleological expedition Son La 1997-1998: Report of the third expedition in the northern provinces of Son La and Lai Chau, SPEKUL, BVKCA, RIGMR, 68 p.

O'Leary, D.W., Friendman, J.D., & Pohn, H.A., 1976, Lineaments, linear, lineation - some proposed new standards for old items: Geological Society of America Bulletin, v. 87, p. 1463-1469.

Sabins, F.F., 1997, Remote Sensing: Principles and interpretation: California, W.H. Freeman and company, 494 p.

Schetselaar, E.M., 2000, Integrated analyses of granite-gneiss terrain from field and multisource remotely sensed data. A case study from the Canadian Shield [PhD thesis]: Technische Universiteit Delft, 269 p.

Schetselaar, E.M., 2001, On preserving spectral balance in image fusion and its advantages for geological image interpretation: Photogrammetric Engineering and Remote Sensing, v. 67, p. 925-934.

SPEKUL, BVKCA, & RIGMR, 2000, Preliminary report of the 4th Vietnamese-Belgian speleological expedition February-March 2000, SPEKUL, BVKCA, RIGMR, 51 pp. & app p.

Szukalski, B.W., 2001, CaveTools version 5.0 for ArcView GIS, http://www.mindspring.com/~bszukalski/cavetools/cavetools.html.

Tam, V.T., Vu, T.M.N., & Batelaan, O., 2001, Hydrogeological characteristics of a karst mountainous catchment in the northwest of Vietnam. Acta geologica sinica (English Edition): Journal of the Geological Society of China, v. 75, no. 3, p. 260-268.

Tien, P.C., An, L.D., Bach, L.D., Bac, D.D., Bosakham Vongdara, Bountheung Phengthavongsa, Danh, T., Dy, N.D., Dung, H.T., Hai, T.Q., Khuc, V., Sauv Chiv Kun, Long, P.D., Mak Ngorn Ly, My, N.Q., Ngan, P.K., Ngoc, N., Nokeo Ratanavong, Quoc, N.K., Quyen, N.V., Somboun Duang Aphaymani, Thanh, T.D., Tri, T.V., Truyen, M.T., & Thach Soval Xay, 1991, Geology of Cambodia, Laos and Vietnam. Explanatory note to the geological map at 1:1,000,000 scale 2nd edition: Hanoi, Geological Survey Vietnam, 158 p.

Tri, T.V., & Tung, N.X., 1979, Geotectonic evolution of northern Vietnam (in Russian): XIV Pacific Scientific Congress, Com. B, Sect. II: Khabarovsk, p. 48-49.

Tri, T.V., Chien, N.V., Cu, L.V., Hao, D.X., Hung, L., Khuc, V., Luong, P.D., Ngan, P.K., Nhan, T.D., Quy, H.H., Thanh, T.D., Thi, P.T., Tho, T., Thom, N., Tung, N.X., & Uy, N.D., 1997, Geology of Vietnam-the north part. Explanatory note to the geological map at 1:1,000,000 scale: Hanoi, Science-Technical Publishing House, 335 p.

Tuyet, D., 1998, Karst geology investigation of the northwest region: Hanoi, Research Institute of Geology and Mineral Resources, 251 p.

Zhang, X.M., Cassells, C.J.S., & Van Genderen, J.L., 1999, Multi-sensor data fusion for the detection of underground coal fires: Geologie en Mijnbouw, v. 77, p. 117-127.